

Disk-Halo-Disk Circulation and the Evolution of the ISM - 3D HD and MHD Adaptive Mesh Refinement Simulations

M.A. de Avillez (1,2), D. Breitschwerdt (2)

(1) *Department of Mathematics, University of Évora, R. Romão Ramalho 59, 7000 Évora, Portugal*

(2) *Institut für Astronomie, Universität Wien, Türkenschanzstr. 17, A-1180 Wien, Austria*

State of the art models of the ISM use adaptive mesh refinement to capture small scale structures, by refining on the fly those regions of the grid where density and pressure gradients occur, keeping at the same time the existing resolution in the other regions. With this technique it became possible to study the ISM in star-forming galaxies in a global way by following matter circulation between stars and the interstellar gas, and, in particular the energy input by random and clustered supernova explosions, which determine the dynamical and chemical evolution of the ISM, and hence of the galaxy as a whole. In this paper we review the conditions for a self-consistent modelling of the ISM and present the results from the latest developments in the 3D HD/MHD global models of the ISM. Special emphasis is put on the effects of the magnetic field with respect to the volume and mass fractions of the different ISM “phases”, the relative importance of ram, thermal and magnetic pressures, and whether the field can prevent matter transport from the disk into the halo. The simulations were performed on a grid with a square area of 1 kpc^2 , centered on the solar circle, extending $\pm 10 \text{ kpc}$ perpendicular to the galactic disk with a resolution as high as 1.25 pc . The run time scale was 400 Myr , sufficiently long to avoid memory effects of the initial setup, and to allow for a global dynamical equilibrium to be reached in case of a constant energy input rate.

Keywords: magneto-hydrodynamics – galaxies: ISM – galaxies: kinematics and dynamics – Galaxy: disk – Galaxy: evolution – ISM: bubbles – ISM: general – ISM: kinematics and dynamics – ISM: structure

1 Introduction

So far our understanding of the evolution of the ISM has been scanty, because of the inherent nonlinearity of all the processes involved. Analytic ISM models, which tried to explain the distribution of the ISM gas into various thermally stable “phases” such as the pioneering work by, e.g., Field (1965), Field et al. (1969), Cox & Smith (1974), and McKee & Ostriker (1977), can at most be regarded as exploratory. Noticeable progress was only possible by the development of sophisticated numerical codes, adequate computing power, and precision input data by observations. Only very recently, by the rapid evolution of telescope and detector technology, as well as the availability of large numbers of parallel processors, we are in the fortunate situation to follow in detail the evolution of the ISM on the global scale taking into account the disk-halo-disk circulation in three dimensions (the first models using 2D grids were developed by Rosen & Bregman 1995).

In this paper we discuss the most important numerical prerequisites for a realistic and self-consistent modelling of the ISM (Section 2), followed by a brief summary of the latest 3D

disk-halo-disk circulation simulations (Section 3). Section 4 discusses model testing and finally, in Section 5 a few final remarks are presented.

2 Modelling of the ISM

The key to a realistic description of the ISM is the use of the appropriate dimensionality, grid coverage, the highest possible spatial resolution, and a realistic input of the basic physical processes with appropriate boundary and initial conditions. All this coupled to the appropriate tools for the included physics, which are sophisticated HD and MHD codes capable of tracking non-linear and small scale structures, solving the Riemann problem between neighbouring cells without introducing large artificial viscosity and guarantee the conservation of $\nabla \cdot \mathbf{B} = 0$ in case magnetic fields are included. These simulations are considered to provide a reliable description of the ISM providing the memory of the initial conditions and evolution has been lost and the models used in these runs have been tested against observations in the local ISM and in particular within the Local Bubble (Cox 2004; Breitschwerdt & Cox 2004, see also Breitschwerdt et al. in this volume).

Dimensionality is of crucial importance as it determines the dynamics (and the turbulence) of the flow with/without magnetic fields. For example, the idea that a disk parallel magnetic field could suppress break-out and outflow into the halo was mainly based on 2D simulations carried out in the last 15 years, owing to computing power limitations. It is obvious, that in 2D-MHD, the flow perpendicular to the magnetic field lines (and hence to the galactic plane) is subject to opposing magnetic tension forces. In 3D however, field lines can be pushed aside and holes and channels can be punched into the gas and field, allowing pressurized flow to circumvent *ever increasing tension and pressure forces* in z -direction.

This behaviour requires that the **grid coverage** in the z -direction must be large enough to accommodate the outflows, whose upper height above the Galactic plane can be estimated by calculating the flow time, τ_f , that the gas needs to travel to the critical point of the flow in a steady-state (see Kahn 1981). This is the characteristic distance from which information in a thermally driven flow can be communicated back to the sources. Then $\tau_f \sim r_c/c_s$, where r_c and c_s are the location of the critical point and the speed of sound, respectively. For spherical geometry, the critical point can be simply obtained from the steady state fluid equations, $r_c \sim GM_{gal}/(2c_s^2)$, which yields with a Milky Way mass of $M_{gal} \approx 4 \times 10^{11} M_\odot$ a distance $r_c \approx 31.3$ kpc for an isothermal gas at $T = 2 \times 10^6$ K (corresponding to a sound speed of $1.67 \times 10^7 \text{ cm s}^{-1}$), and thus $\tau_f \sim 180$ Myr as an upper limit for the flow time. For comparison, the radiative cooling time of the gas at a typical density of $n = 2 \times 10^{-3} \text{ cm}^{-3}$ is roughly $\tau_c \sim 3k_B T/(n\Lambda) \approx 155$ Myr for a standard collisional ionization equilibrium cooling function $\Lambda = 8.5 \times 10^{-23} \text{ erg cm}^3 \text{ s}^{-1}$ of gas with cosmic abundances. This value is apparently of the same order as the flow time, ensuring that the flow will not only cool by adiabatic expansion, but also radiatively, thus giving rise to the fountain return flow, which is the part of the outflow that loses pressure support from below and therefore cannot escape. Note that r_c is the maximum extension of the fountain flow in steady state. Thus, the lack of such an extended z -grid inhibits the disk-halo-disk circulation of matter, which otherwise would return gas to the disk sometime later, with noticeable effects for the dynamical evolution there. The loss of matter may be compensated by some injection of mass by means of rather artificial **boundary conditions** imposed into the upper and bottom faces of the grid.

The **resolution** adopted in a simulation results from a compromise between the available computing resources and the minimum scale required to handle appropriately the physical processes involved in the system under study. For instance in the ISM simulations high resolutions are required due to the formation of small scale structures, resulting from instabilities in the flows, in particular from thermal instabilities and condensations as a result of radiative cool-

ing. The amount of cooling may be substantially increased if the resolution is high enough to trace regions of high compression by shocks, rather than smearing them out over larger cells, and thereby wiping out density peaks. Radiative cooling as a nonlinear process can become more efficient, since high density regions contribute more to the energy loss rate than low density regions can compensate by an accordingly lower rate. Since cooling is most efficient for dense gas, the cool phase is affected most. In addition, the spatial resolution of shear layers and contact surfaces, gives rise to an increased level of turbulence and a larger number of mixing layers. The latter is most important, because it allows for a faster mixing between parcels of gas with different temperatures (conduction or diffusion processes being of second order and hence inherently slow in nature). The small scale mixing is promoted by numerical rather than molecular diffusion, and therefore, the time scales for mixing in the different phases to occur is somewhat smaller (because it happens on larger scales) than those predicted by molecular diffusion theory (e.g., Avillez & Mac Low 2002). However, turbulent diffusion, as a consequence of the onset of turbulence due to shear flows, will be most efficient.

A necessary, but not sufficient, condition on **convergence** of the simulations is that by increasing the resolution (normally by doubling it a few times) global properties, such as volume filling factors, history of minimum temperature and maximum density, mass distribution with time, etc, do not change significantly. When the numerical solutions, with the increase in resolution, have a small discrepancy of a few percent then one can safely conclude that the simulations converge for the physical processes included. For further discussion see Avillez & Breitschwerdt (2004).

The initial evolution of a system imprints its signature in the averaged histograms of time evolved variables until the nonlinear processes developing during this time wipe out the signature of the initial conditions. In the case of global models as the ones discussed below, the initial evolution imprint is still seen after 70 Myr of evolution of a magnetized ISM (Fig. 1, which shows averaged volume weighted histograms of the temperature over the periods of 0-50, 20-70 and 350-400 Myr for an MHD run with the Galactic SN rate and a finest AMR resolution of 1.25 pc). This imprint is also seen in corresponding histograms of HD simulations (Avillez & Breitschwerdt 2004).

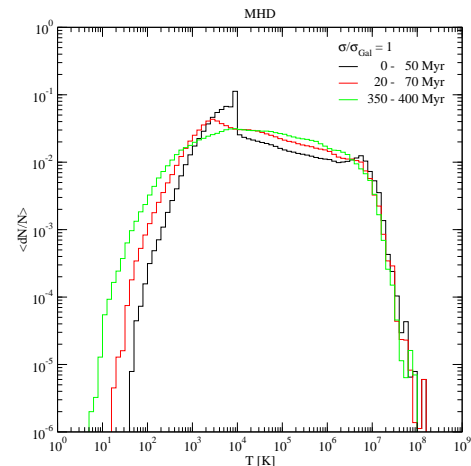


Figure 1: Averaged volume-weighted temperature histogram for a MHD global ISM simulation over the periods of 0-50 Myr (black), 20-70 Myr (red) and 350-400 Myr (green) calculated using 51 snapshots taken at time intervals 1 Myr. The resolution of the finest AMR level is 1.25 pc.

3 Results from the Latest HD and MHD Simulations of a Disk-halo-disk Circulation System

Taking into account the above considerations we carried out high resolution (using adaptive mesh refinement with finer resolutions ranging from 0.625 to 2.5 pc and coarse grid resolution of 10 pc) three-dimensional kpc-scale HD and MHD simulations of the ISM including the disk-halo-disk circulation with a grid centred on the solar circle and extending from $z = -10$ to 10 kpc with a square disk area of 1 kpc². The basic processes included are the gravitational field provided by the stars in the disk, radiative cooling assuming an optically thin gas in collisional ionization equilibrium, uniform heating due to starlight varying with z , supernovae (with a canonical explosion energy of 10^{51} erg) types Ia (with scale height, distribution and rate taken

from the literature) and Ib and II, whose formation, and spatial location is calculated self-consistently by determining the number and masses and main sequence lifetimes of the OB stars formed in regions with $n \geq 10 \text{ cm}^{-3}$, $T \leq 100 \text{ K}$, respectively, and $\nabla \cdot \vec{v} < 0$, where \vec{v} is the gas velocity. Some 40 – 50% of the stars (these are mainly the stars with masses $\leq 11M_{\odot}$) explode in the field (the rest in associations) and have an average scale height of $\sim 90 \text{ pc}$. The mean total rate per unit volume of occurrence of SNe in these simulations is $18 \text{ kpc}^{-3} \text{ Myr}^{-1}$, a value similar to the observed one. In the case of the MHD run the ISM is pervaded by a magnetic field with a total strength of $\simeq 4.45 \mu\text{G}$ resulting from uniform and random components with mean values of 3.25 and $3.1 \mu\text{G}$, respectively.

3.1 Global Evolution

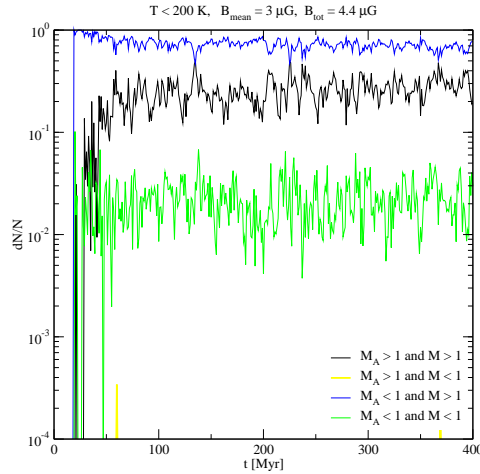
The simulations depart from an hydrostatic setup of the disk and halo gas which does not hold for long as a result of the lack of equilibrium between gravity and (thermal, kinetic and turbulent) pressure during the “switch-on phase” of SN activity. As a consequence the gas in the upper and lower parts of the grid collapses onto the midplane, leaving low density material behind. However, in the MHD run it takes a longer time for the gas to descend towards the disk and the complete collapse into the midplane is prevented by the opposing magnetic pressure and tension forces. As soon as enough SNe have gone off in the disk building up the required pressure support, a thick frothy disk is formed overlayed by a hot halo. The thick gas disk is feeded and supported by the motions of the hot gas warmed up by randomly distributed SNe which rises buoyantly and eventually breaks through into the halo. Transport into the halo is not prevented, although the escape of the gas takes a few tens of Myr to occur in the MHD run – somewhat longer than in the pure hydrodynamical case. The crucial point is that the huge thermal overpressure due to combined SN explosions can sweep the magnetic field into dense filaments and punch holes into the extended warm and ionized layers allowing the setup of pressure release valves, after which there is no way from keeping the hot over-pressured plasma to follow the pressure and density gradient into the halo.

Fig. 2 shows the density distribution in the plane perpendicular to the Galactic midplane at time 166 Myr. Red/blue in the colour scale refers to lowest/highest density (or highest/lowest temperature). The z -scale above 0.5 and below -0.5 kpc is shrunk (in order to fit the paper size) and thus, the distribution of the labels is not uniform. The image shows the presence of a wiggly thin disk

Jpeg image fig2.jpg

Figure 2: Slice through the 3D data set showing the vertical (perpendicular to the midplane) distribution of the density at time 166 Myr.

of cold gas overlaid by a frothy thick disk (punctured by chimneys and crossed by hot buoyant ascending gas) composed of neutral (light blue), with a scale height of ~ 180 pc, and ionized (greenish) gas with a scale height of 1 kpc. These distributions reproduce those described in Dickey & Lockman (1990) and Reynolds (1987), respectively. The upper parts of the thick ionized disk form the disk-halo interface located around 2 kpc above and below the midplane, where a large scale fountain is set up by hot ionized gas, injected there either from gas streaming out of the thick disk or directly from superbubbles in the disk underneath, escaping in a turbulent convective flow. The corresponding magnetic field maps, presented in Avezil & Breitschwerdt (2005), show the presence of a thin magnetized disk overlaid by Parker-like loops (produced without cosmic rays), magnetic islands, and clouds wrapped in field lines moving downwards. There is also cold gas descending along the Parker loops.



Jpeg image fig3b.jpg

Figure 3: *Left panel:* History of the cold ($T \leq 200$ K) gas fraction that is super/sub-alfvénic (denoted by $M_A > or < 1$) and super/sub-sonic (denoted by $M > or < 1$). As it can be seen the less than $10^{-2}\%$ of cold gas has $M_A > 1$ and $M < 1$. *Right panel:* Scatter plot of B versus n for $T \leq 10^2$ (black), $10^2 < T \leq 10^{3.9}$ (grey), $10^{3.9} < T \leq 10^{4.2}$ (blue), $10^{4.2} < T \leq 10^{5.5}$ K (green), and $T > 10^{5.5}$ K (red) regimes at 400 Myr of disk evolution. The points in the plot are sampled at intervals of four points in each direction.

3.2 Shock Compressed Layers

The highest density gas with $T \leq 10^2$ K is confined to shocked compressed layers that form in regions where several large scale streams of convergent flow (driven by SNe) occur. The compressed regions, which have on average lifetimes of a few free-fall times, are filamentary in structure, tend to be aligned with the local field and are associated with the highest field strengths (in the MHD run), while in the HD runs there is no preferable orientation of the filaments. The formation time of these structures depends on how much mass is carried by the convergent flows, how strong the compression and what the rate of cooling of the regions under pressure are. During the dynamical equilibrium evolution on average 70% of the cold ($T \leq 200$ K) gas is subalfvénic and supersonic, while only 1-5% is subalfvénic and subsonic, the remaining fraction of the gas has $M_A > 1$ and $M > 1$ (Fig. 3). This means that although in the ISM the majority of the cold gas is supersonic and subalfvénic there is a considerable fraction ($\langle dN/N \rangle \simeq 30\%$) of the gas where the mean magnetic pressure is dynamically low, i.e., $M_A > 1$.

3.3 Field Dependence with Density

After the global dynamical equilibrium has been set up the magnetic field shows a high variability (which decreases towards higher gas densities spanning two orders of magnitude from 0.1 to 15

μG ; see Fig. 3) and it is *largely uncorrelated with the density*. The spreading in the field strength increases with temperature, being largest for the hot ($T > 10^{5.5}$ K) and smallest (with almost an order of magnitude variation from 0.8 to 6 μG) for the cold ($T \leq 200$ K) gas. The large scatter in the field strength for the *same* density, seen in Fig. 3, suggests that the field is being driven by the inertial motions, rather than it being the agent determining the motions. In the latter case the field would not be strongly distorted, and it would direct the motions predominantly along the field lines. In ideal MHD field diffusion is negligible, and the coupling between matter and field should be perfect (we are of course aware of numerical diffusion which weakens the argument at sufficiently small scales). Therefore gas compression is correlated with field compression, except for strictly parallel flow.

3.4 Driving Forces in the ISM

The relative importance of the driving pressures, i.e., thermal (P_{th}), ram (P_{ram}) and magnetic (P_{mag}), in the ISM varies with increasing temperature (Fig. 4). For $T \leq 150$ K $P_{\text{th}} \ll P_{\text{ram}} < P_{\text{mag}}$ indicating that the gas is dominated by the Lorentz $\vec{j} \times \vec{B}$ force, and the magnetic field determines the motion of the fluid, while for $T \geq 10^{5.5}$ K thermal pressure dominates. At the intermediate temperatures ram pressure determines the dynamics of the flow, and therefore, the magnetic pressure does not act as a significant restoring force (see Pasot & Vázquez-Semadeni 2003) as it was already suggested by the lack of correlation between the field strength and the density. It is also noteworthy that in this temperature range (150 – $10^{5.5}$ K) the weighted magnetic pressure is roughly constant (suggesting that the magnetic and thermal pressures are largely independent, whereas both thermal and ram pressures undergo large variations in this temperature interval).

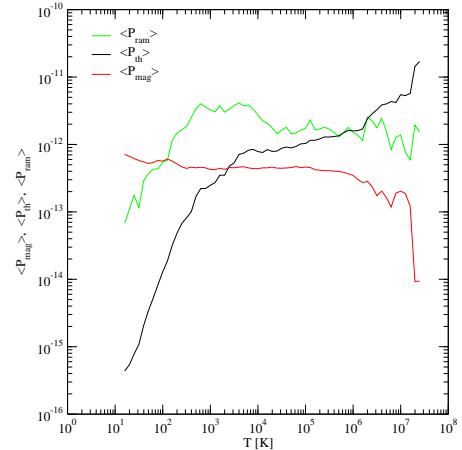


Figure 4: Average $\langle P_{\text{ram}} \rangle$ (green), $\langle P_{\text{th}} \rangle$ (black), and $\langle P_{\text{mag}} \rangle$ (red) as function of the temperature (in the simulated disk $|z| \leq 250$ pc) averaged over temperature bins of $\Delta \log T = 0.1$ K between 350 and 400 Myr.

3.5 The Chandrasekhar-Fermi Law

As ram pressure fluctuations in the ISM dominate over the other pressures a perfect correlation between the field and density following the classical scaling law $B \sim \rho^\alpha$ is not expected, with $\alpha = 1/2$, according to the Chandrasekhar-Fermi (CF) model (1953), but a broad distribution of B versus ρ . Although in general $0 \leq \alpha \leq 1$ would be expected, it should be noted that in reality heating and cooling processes, and even magnetic reconnection could induce further changes, making the correlation rather complex. It should be kept in mind that in CF it was assumed that the field is distorted by turbulent motions that were subalfvénic, whereas in our simulations in addition both supersonic and superalfvénic motions can occur, leading to strong MHD shocks. In other words, according to the CF model, the turbulent velocity is directly proportional to the Alfvén speed, which in a SN driven ISM need not be the case.

3.6 Pressure Distributions and Fluctuations

The pressure coverage of three orders of magnitude, for volume fractions of $dN/N \geq 10^{-2}$, seen in the averaged (over the period 350-400 Myr) volume weighted histograms of P_{th} (Fig. 5) is similar

for the magnetized and unmagnetized ISM runs, although the power law fits to their profiles have different negative slopes: 2.6 and 1.5, respectively. These results are indicative of the large fluctuations in thermal pressure between different temperature regimes, suggesting that there are no real "phases", i.e., co-existing thermodynamic regimes with different density and temperature but in pressure equilibrium (see also Avillez & Breitschwerdt 2004, 2005; Mac Low et al. 2005).

3.7 Volume Weighted Histograms

A comparison between the averaged (over the time 350 through 400 Myr) volume weighted histograms of the density and temperature of the magnetized and unmagnetized disk gas shows differences that include the (i) decrease/increase by an almost order of magnitude in the histograms density/temperature coverage, (ii) change in the relative weight of the dominant temperature regimes (in the density histograms) and consequently (iii) changes in the pronounced bimodality of the total density and temperature histograms. This latter effect is most noticeable in the temperature PDFs (see Fig. 1). In effect, while the temperature PDF of the HD run has a bimodal structure (as it has two peaks: one at 2000 K and another around 10^6 K), in the MHD run the decrease/increase in importance of the $10^{3.9} < T \leq 10^{4.2}$ K/ $10^{4.2} < T \leq 10^{5.5}$ K leads to the reduction/increase of the occupation fraction of these regimes and therefore to a change of the histogram structure appearing it to be unimodal. This variation of the intermediate region appears to be an effect of the presence of the magnetic field, with the smoothing effect being less pronounced for lower field strengths in the disk.

3.8 Volume Filling Factors

During most of the history ($t > 100$ Myr) of ISM evolution the occupation (f_V) fractions of the different thermal regimes have an almost constant distribution, varying around their mean values (cf. Table 1; see also Avillez 2000; Avillez & Breitschwerdt 2004, 2005). The thermally stable regimes with $T \leq 200$ K and $10^{3.9} < T \leq 10^{4.2}$ K have similar occupation fractions of $\sim 5\%$ and $\sim 10\%$, respectively, in both runs, while the hot gas has an increase from $\sim 17\%$ in the HD run to $\sim 20\%$ in the MHD case. By far the disk volume is occupied by gas in the thermally unstable regimes at $200 < T \leq 10^{3.9}$ and $10^{4.2} < T \leq 10^{5.5}$ K with similar occupation fractions $\sim 30\%$ in the MHD run, while in the HD run these regimes occupy 46% and 22%, respectively, of the disk volume.

These results indicate that the presence of the magnetic field, which may inhibit the breakout of an individual remnant, but certainly not the high-pressure flow resulting from supernova explosions in concert within an OB association, only leads to a slight increase in the occupation fraction of the hot gas in the disk. The reason is that the volume filling factor of the hot gas increases slightly because magnetic tension forces help to confine bubbles and Lorentz forces obstruct mixing with cooler gas. It is plausible to assume that, similarly to what seen in HD simulations with different star forming rates, there is a correlation between the filling factor of

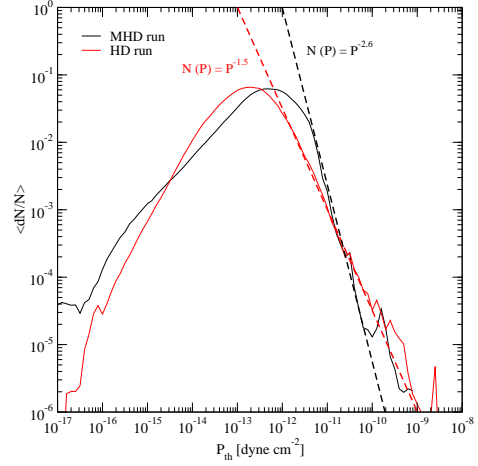


Figure 5: Averaged thermal pressure distribution in the simulated disk ($|z| \leq 250$ pc) for the MHD (black) and HD (red) runs. These pdfs are calculated by using 51 snapshots taken between 350 and 400 Myr with a time interval of 1 Myr. The right side of the histograms is overlaid with a straight dashed line corresponding to power laws with negative slopes 1.5 and 2.6.

the hot gas and the rate at which SN occur, since higher rates will produce more hot plasma which, as we have shown here, is not magnetically controlled.

Table 1: Summary of the average values of volume filling factors, mass fractions and root mean square velocities of the disk gas at the different thermal regimes for the HD and MHD runs (from Avillez & Breitschwerdt 2005).

T [K]	$\langle f_V \rangle^a$ [%]		$\langle f_M \rangle^b$ [%]		$\langle v_{\text{rms}} \rangle^c$	
	HD	MHD	HD	MHD	HD	MHD
< 200 K	5	6	44.2	39.9	7	10
200 – $10^{3.9}$	46	29	49.0	43.7	15	15
$10^{3.9}$ – $10^{4.2}$	10	11	4.4	8.5	25	21
$10^{4.2}$ – $10^{5.5}$	22	33	2.0	7.4	39	28
> $10^{5.5}$	17	21	0.3	0.5	70	55

^a volume filling factor.

^b Mass fraction.

^c Root mean square velocity in units of km s^{-1} .

3.9 ISM Mass Fractions and Warm Neutral Medium Mass

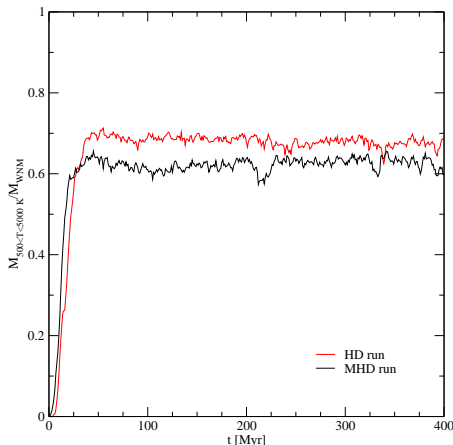


Figure 6: History of the fraction of mass of the WNM gas having $500 < T \leq 5000$ K in the disk for the HD (red) and MHD (black) runs.

Most of the disk mass is found in the $T \leq 10^{3.9}$ K gas, with the cold ($T \leq 200$ K) and thermally unstable gases ($200 < T \leq 10^{3.9}$ K) harbouring on average 80 and $\sim 90\%$ of the disk mass in the MHD and HD runs (Table 1), with the cold regime enclosing $\sim 40\%$ of the disk mass. The remaining ISM mass is distributed between the other temperature regimes with the $10^{3.9} < T \leq 10^{4.2}$ K and $10^{4.2} < T \leq 10^{5.5}$ K regimes enclosing a total of only $\sim 7\%$ and $\sim 16\%$ of mass in the HD and MHD runs, respectively, and the hot gas enclosing $< 1\%$ of the disk mass in both runs. In both runs, 60-70% of the warm neutral mass ($500 < T \leq 8000$ K) is contained in the $500 \leq T \leq 5000$ K temperature range (bottom panel of Fig. 6).

This latter result is strongly supported by interferometric (Kalberla et al. 1985) and optical/UV absorption-line measurements (Spitzer & Fitzpatrick 1995, Fitzpatrick & Spitzer 1997), which indicate that a large fraction ($\sim 63\%$) of the warm neutral medium (WNM) is in the unstable range $500 < T < 5000$ K. Moreover 21 cm line observations (Heiles 2001; Heiles & Troland 2003) provide a lower limit of 48% for the WNM gas in this unstable regime. Direct numerical simulations of the nonlinear development of the thermal instability under ISM conditions with radiative cooling and background heating discussed in Gazol et al. (2001) and Kritsuk & Norman (2002) show that about 60% of the system mass is in the thermally unstable regime. However, it is unclear from their simulations what the time evolution of this mass fraction (which is shown in the figure for $t > 100$ Myr) is and what explicitly the origin of the unstable gas is. These authors suggest that ensuing turbulence is capable of replenishing gas in the thermally unstable regime by constantly stirring up the ISM. We have carried out detailed numerical studies of the stability of the ISM gas phases (Avillez & Breitschwerdt 2005a), and verified the hypothesis that SN driven turbulence is capable of replenishing fast cooling gas in classically

unstable regimes. In effect, turbulence as a diffusion process can prevent thermal runaway on small scales. That is, turbulence has a stabilizing effect thereby inhibiting local condensation modes. The turbulent viscosity $\nu_{\text{turb}} \sim Re \nu_{\text{mol}}$ can be orders of magnitude above the molecular viscosity, with Re being the Reynolds number of the flow. What happens physically then, is that with increasing eddy wavenumber $k = 2\pi/\lambda$, the eddy crossing time $\tau_{\text{eddy}} \sim \lambda/\Delta u$ (with Δu being the turbulent velocity fluctuation amplitude) becomes shorter than the cooling time $\tau_{\text{cool}} \sim 3k_B T/(n\Lambda(T))$, where $\Lambda(T)$ is the interstellar cooling function. Although not strictly applicable here, it is instructive to see that in case of incompressible turbulence following a Kolmogoroff scaling law, where the energy dissipation rate is given by $\varepsilon \sim \rho \Delta u^3/\lambda$, we obtain a lower cut-off in wavelength, where thermal instability becomes inhibited, if

$$\begin{aligned} \lambda &< \left(\frac{3k_B \bar{m}}{\Lambda_0} \right)^{3/2} \varepsilon^{1/2} \frac{T^{3/4}}{\rho^2} \\ &\approx 1.4210^{19} \text{ cm}, \end{aligned} \quad (1)$$

taking $\varepsilon \sim 10^{-26} \text{ erg cm}^{-3} \text{ s}^{-1}$ for SN energy injection; a simple cooling law for the warm neutral medium of $\Lambda(T) = \Lambda_0 T^{1/2}$ has been adopted, with $\Lambda_0 \approx 1.9 \times 10^{-27} \text{ erg cm}^3 \text{ s}^{-1} \text{ K}^{-1/2}$ (taken from the cooling curve of Dalgarno & McCray 1972) for a WNM of a density of $n = 0.3 \text{ cm}^{-3}$, a temperature of $T = 1000 \text{ K}$, and a low degree of ionization $x \approx 0.01$. Therefore rough numerical estimates are typically of the order of parsecs, consistent with our numerical resolution. In fact, the critical wavelength λ varies with temperature, degree of ionization and hence cooling; for the WNM we find quite a large range of values from $10^{17} - 10^{20} \text{ cm}$, according to Eq. (1).

3.10 Turbulent Velocities

The root mean square velocity, V_{rms} , which is a measure of the disordered motion of the gas, increases with temperature (see Table 1) in the MHD and HD runs. The average rms velocity ($\langle V_{\text{rms}} \rangle$) in the last 100 Myr of evolution has large fluctuations in the different thermal regimes in the HD run, which are reduced due to the presence of the magnetic field. These velocities agree remarkably well with the observed rms velocities discussed by Kulkarni & Fich (1985). The near constancy of the rms velocity with time indicates the presence of a dynamical equilibrium, with random motions, i.e. thermal and turbulent pressures adding to the total pressures, provided that the energy injection rate remains constant on a global scale.

4 Testing the Model

Although the above mentioned results are in good agreement with present day observations of the ISM and other numerical experiments, though these have more a local character, one can trace the quality of the present model by applying it to the dynamics and evolution of the Local Bubble, powered by the explosions of 19 SNe in the last 14 Myr (Berghöfer & Breitschwerdt 2002; Fuchs et al. 2005), and trace its OVI content that has been observed using Copernicus and FUSE. While standard Local Bubble (LB) models fail to reproduce the observed low OVI absorption column density (Shelton & Cox 1994; for a recent discussion see Breitschwerdt & Cox 2004), the present model when applied to the study of the dynamics and evolution of the Local and Loop I bubbles predicts column densities $< 1.7 \times 10^{13} \text{ cm}^{-2}$ towards Loop I with a mean value of $\leq 8.5 \times 10^{12} \text{ cm}^{-2}$ (for details see Breitschwerdt et al. these proceedings) in agreement with the mean column density of $7 \times 10^{12} \text{ cm}^{-2}$ inferred from analysis of FUSE absorption line data in the Local ISM (Oegerle et al. 2004).

5 Final Remarks

The present simulations still neglect an important component of the ISM, i.e., high energy particles, which are known to be in rough energy equipartition *locally* with the magnetic field, the thermal and the turbulent gas in the ISM. The presence of CRs and magnetic fields in galactic halos is well known and documented by many observations of synchrotron radiation generated by the electron component. The fraction of cosmic rays that dominates their total energy is of Galactic origin and can be generated in SN remnants via the diffusive shock acceleration mechanism to energies up to 10^{15} eV (for original papers see Krymski et al. 1977, Axford et al. 1977, Bell 1978, Blandford & Ostriker 1978, for a review Drury 1983, for more recent calculations see Berezhko 1996). The propagation of these particles generates MHD waves due to the streaming instability (e.g. Kulsrud & Pearce 1969) and thereby enhances the turbulence in the ISM. In addition, self-excited MHD waves will lead to a dynamical coupling between the cosmic rays and the outflowing fountain gas, which will enable part of it to leave the galaxy as a galactic wind (Breitschwerdt et al. 1991, 1993, Dorfi & Breitschwerdt 2005). Furthermore, as the cosmic rays act as a weightless fluid, not subject to radiative cooling, they can bulge out magnetic field lines through buoyancy forces. Such an inflation of the field will inevitably lead to a Parker type instability, and once it becomes nonlinear, it will break up the field into a substantial component parallel to the flow (Kamaya et al. 1996), thus facilitating gas outflow into the halo. We are currently performing ISM simulations including the CR component.

In the dynamical picture of the ISM emerging from our simulations, thermal pressure gradients dominate mainly in the neighbourhood of SNe. These events drive motions whose ram pressures overwhelm the mean thermal pressure (away from the energy sources) and the magnetic pressure by a large factor. The magnetic field is dynamically important at low temperatures, apart from also weakening gas compression in MHD shocks and thereby lowering the energy dissipation rate. The thermal pressure of the freshly shock heated gas exceeds the magnetic pressure by usually more than an order of magnitude and the B-field can therefore not prevent the flow from rising perpendicular to the galactic plane. Thus hot gas is fed into the galactic fountain at almost a similar rate than without field (Avillez & Breitschwerdt 2004, 2005).

However, the circulation of gas between the disk and halo is a dynamic process, which involves a flow time scale, that can be much shorter than any of the microphysical time scales due to ionization and recombination. The gas escaping into the halo has an initial temperature well in excess of 10^6 K, where the assumption of collisional ionization equilibrium (CIE) is approximately valid. This means that the rate of ionizations per unit volume through collisions between ions and electrons equals the rate of recombinations per unit volume. As the hot plasma expands away from the disk it will cool adiabatically thereby reducing its temperature and density. It has been shown (Breitschwerdt & Schmutzler 1999) that recombination of highly ionised species lags behind and occurs mainly at considerable heights from the disk. In the case of the X-ray halo of NGC 3029, spectral fitting has shown that an outflow model based on non-equilibrium ionization (NEI) effects gives an excellent agreement with observations (see Breitschwerdt 2003).

Acknowledgments

MA would like to thank the SOC and Thierry Montmerle and Almas Chalabaev for the invitation and financial help to attend this excellent conference.

References

1. Avillez, M. A. 2000, MNRAS, 315, 479

2. Avillez, M. A., & Mac Low, M.-M. 2002, ApJ, 581, 1047
3. Avillez, M. A., & Breitschwerdt, D. 2004, A&A, 425, 899
4. Avillez, M. A., & Breitschwerdt, D. 2005a, A&A, in press
5. Avillez, M. A., & Breitschwerdt, D. 2005b, ApJ, in preparation
6. Axford, W.I., Leer, E., & Skadron, G. 1977, in Proc. 15th Int. Cosmic Ray Conf. (Plodiv) 11, 132
7. Bell, A. R. 1978, MNRAS, 182, 147
8. Berezhko, E. G. 1996, APh 5, 367
9. Berghöfer, T., & Breitschwerdt, D. 2002, A&A, 390, 299
10. Blandford, R. D., & Ostriker, J. P. 1978, ApJ, 221, 29
11. Breitschwerdt, D., McKenzie, J.F., & Völk, H.J. 1991, A&A 245, 79
12. Breitschwerdt, D., McKenzie, J.F., & Völk, H.J. 1993, A&A 269, 54
13. Breitschwerdt D., & Schmutzler T. 1999, A&A, 347, 650
14. Breitschwerdt D. 2003, RMxAA (Serie de Conferencias), 15, 311
15. Breitschwerdt, D., & Cox, D. P. 2004, in "How does the Galaxy Work?", eds. E. Alfaro, E. Perez, & J. Franco, Kluwer (Dordrecht), p. 391
16. Chandrasekhar, S., & Fermi, E. 1953, ApJ, 118, 113
17. Cox, D. P., & Smith, B. W. 1974, ApJ, 189, L105
18. Cox, D. P. 2004, in "From Observations to Self-consistent Modelling of the ISM in Galaxies", eds. M. A. de Avillez, & D. Breitschwerdt, Kluwer (Dordrecht), p.
19. Dalgarno, A., & McCray, R. A. 1972, ARA&A, 10, 375
20. Dickey, J. M., & Lockman, F. J. 1990, ARA&A, 28, 215
21. Dorfi, E.A., Breitschwerdt, D. 2005, A&A (in preparation)
22. Drury, L. O'C. 1983, Rep. Prog. Phys. 46, 973
23. Field, G. B. 1965, ApJ, 142, 531
24. Field, G. B., Goldsmith, D. W., & Habing, H. J. 1969, ApJ, 155, L149
25. Fitzpatrick, E. L., & Spitzer, L. 1997, ApJ, 475, 623
26. Fuchs, B., Breitschwerdt, d., Dettbarn, C., & Flynn, C. 2005, MNRAS, in preparation
27. Gazol, A., Vázquez-Semadeni, E., Sanchez-Salcedo, J., & Scalo, J. 2001, ApJ, 557, 121
28. Heiles, C. 2001, ApJ, 551, L105
29. Heiles, C., & Troland, T. H. 2003, ApJ, 586, 1067
30. Kalberla, P. M. W., Schwarz, U. J., & Goss, W. M. 1985, A&A, 144, 27
31. Kamaya, H., Mineshige, S., Shibata, K., & Matsumoto, R. 1996, ApJ, 458, L25
32. Kahn, F. D. 1981, in "Investigating the Universe", ed. F.D. Kahn, Reidel (Dordrecht), p. 1.
33. Kritsuk, A., & Norman, M. L. 2002, ApJ, 580, L51
34. Krymsky, G. F. 1977, Dokl. Nauk. SSR 234, 1306, (Engl. trans. Sov. Phys. Dokl. 23, 327)
35. Kulsrud, R. M., & Pearce, W. D. 1969, ApJ, 156, 445
36. Mac Low, M.-M., Balsara, D., Kim, J., & Avillez, M. A. 2004, ApJ, in revision [astro-ph/0410734]
37. McKee, C. F., Ostriker, J. P. 1977, ApJ 218, 148
38. Oegerle, W. R., E. B. Jenkins, E. B., Shelton, R. L., Bowen, D. V., & Chayer, P. 2005, ApJ, Submitted [astro-ph/0411065]
39. Passot, T., Vázquez-Semadeni, E. 2003, A&A, 398, 845
40. Reynolds R. J. 1987, ApJ, 323, 118
41. Rosen A., & Bregman, J. N. 1995, ApJ, 440, 634
42. Shelton, R., & Cox, D. P. 1994, ApJ, 434, 599
43. Spitzer, L., & Fitzpatrick, E. L., 1995, 445, 196

This figure "fig3b.jpg" is available in "jpg" format from:

<http://arxiv.org/ps/astro-ph/0502078v1>